

## Construction of a Wide tuneable Volume Coil for Small-Animal MR Imaging

M. Vít<sup>a,b</sup>, M. Burian<sup>a</sup>, A. Gálisová<sup>a</sup>, D. Jiráček<sup>a,b\*</sup>

<sup>a</sup>Institute for Clinical and Experimental Medicine, Videňská 1958/9, 140 21 Praha 4, Czech Republic

<sup>b</sup>Technical university of Liberec, Studentská 1402/2, 461 17 Liberec, Czech Republic

Corresponding Author: D. Jiráček

---

**Abstract:** We present a radio frequency volume coil with a working volume of 100 ml for in vivo <sup>1</sup>H and <sup>19</sup>F MR imaging of small rodents using a 4.7 T experimental spectrometer. Equipped with single-channel excitation, the coil has a birdcage structure with twelve longitudinal elements to generate a sufficiently homogeneous B<sub>1</sub> electromagnetic field in the coil. In contrast to commonly constructed birdcage coils, our coil can change the resonant frequency over a large frequency range (including  $f_{019F} = 188.6 \text{ MHz}$  -  $f_{01H} = 200.4 \text{ MHz}$  @ B<sub>0</sub> 4.7 T) by adjusting the electrical capacitance between wires to reflect changes in the length of the coil. The quality factors of the resonances in an unloaded coil are Q<sub>1H</sub> = 328 and Q<sub>19F</sub> = 331, which are comparable to a standard birdcage coil design used for only one of the frequencies. However, this novel coil enables measurement of <sup>1</sup>H as well as <sup>19</sup>F images with comparable MR signals, and dispenses with the need to adjust coils between individual measurements. This means both measurements can be taken for identical rodent positions.

**Keywords:** molecular imaging, small animals, magnetic resonance imaging, birdcage coil, <sup>1</sup>H/<sup>19</sup>F MRI

---

Date of Submission: 25-06-2019

Date of acceptance: 10-07-2019

---

### I. Introduction

Magnetic resonance (MR) imaging plays an important role in both preclinical and clinical research. Animal model experiments are an essential tool for examining various diseases and determining potential treatment options. Most of these experiments are conducted on mice. The average body size of a mouse is around 2 to 3 cm from neck to tail root. For imaging rodents of this size, high contrast imaging equipment is therefore required [1]. In general, most commercially available universal radiofrequency (RF) coils are not adapted for mouse whole-body imaging due to the different sizes of rodent bodies. As mice are small in size, sensitivity can be impacted, resulting in a low signal-to-noise ratio (SNR). A very important property of the RF coil is the homogeneity of its magnetic field (B<sub>1</sub>), which is necessary for whole-body MR imaging (MRI), MR relaxometry and MR spectroscopy (MRS). Volume coils receive MR signals from the whole inside volume and generally produce a highly homogeneous B<sub>1</sub> field.

In this work, we present a new design for a sensitive radiofrequency volume coil (volume of interest at ~ 100 ml) intended for in vivo <sup>1</sup>H/<sup>19</sup>F MR whole-body imaging and spectroscopy in small rodents using a 4.7 T experimental spectrometer.

Among the most commonly used and suitable volume coils for transmitting and receiving MR signals (Tx/Rx– transceiver) are the saddle coil, the solenoid, the birdcage, and the transverse electromagnetic wave resonator (TEM). The electromagnetic (EM) field of the saddle coil is characterised by low homogeneity, while the coil axis of the solenoid needs to be oriented perpendicular to the static magnetic field (B<sub>0</sub>), a limitation for small-bore animal systems due to animal positioning. The design of the TEM is generally not suitable for static magnetic fields lower than 5T [2].

The optimal volume transceiver coil remains the birdcage coil. It has a reliably homogeneous B<sub>1</sub> field, a reasonably accessible inner volume, and can be relatively easily fabricated in a standard equipped laboratory. For low static magnetic fields (<5 T) or smaller specimen sizes (experimental settings), the low pass type is recommended due to construction reasons. However, high pass (HP) or band pass (BP) types can also be used. Particular construction types differ with regard to the disposition of components and the spectra of resonance modes [2]. The standard birdcage volume coil is widely acknowledged to be the one-channel volume coil, as described previously [2].

Conventionally, coils are constructed from conductor sections possessing inductance (L) and from capacitors with lumped parameters representing capacity (C). The capacitors must be non-magnetic so as not to disturb the homogeneity of the magnetic field. They also account for a significant part of the cost of the coil (Table1).

Clinical and experimental MRI mostly measures signals from the hydrogen  $^1\text{H}$  isotope. However, MR-active nuclei such as fluorine  $^{19}\text{F}$ , phosphorus  $^{31}\text{P}$ , sodium  $^{23}\text{Na}$  and carbon  $^{13}\text{C}$  represent further interesting targets for imaging and spectroscopic MR techniques [3]. MRI probes based on fluorinated compounds have proved highly promising [4, 5, 6, 7, 8]. The Larmor frequency of  $^{19}\text{F}$  is relatively close to that of  $^1\text{H}$ , which means that even some commercial MR scanners can be used for  $^{19}\text{F}$  MRI after introducing only minor hardware and software changes [9]. Another advantage of  $^{19}\text{F}$  MRI is that it only exhibits a negligible fluorine background in living tissue. Therefore,  $^{19}\text{F}$  MR provides high specificity and “hot spot” imaging, where the  $^{19}\text{F}$  MR image is overlaid on a  $^1\text{H}$  reference MR image. Another benefit of  $^{19}\text{F}$  MR is that absolute quantification of  $^{19}\text{F}$  content is easy to achieve, since the fluorine signal detected is directly proportional to the number of  $^{19}\text{F}$  nuclei. This favours the use of fluorinated compounds as a potent tool for preclinical or even clinical imaging [10]. The main disadvantage of  $^{19}\text{F}$  MR is its low sensitivity due to both the small amount of  $^{19}\text{F}$  nuclei per molecule of the synthesised fluorine-based probes and their low concentration (units of millimoles) [11]. However, this limitation can be overcome by using a high magnetic  $B_0$  field or sensitive RF receiver circuits. Coils for  $^1\text{H}$  imaging typically require only a narrow tuning range, if at all. Gyromagnetic ratios of  $^{19}\text{F}$  and  $^1\text{H}$  differ by about 6%. Larmor frequencies for magnetic field 4.7 T correspond to  $f^1_{\text{H}} = 200.4$  MHz and  $f^{19}_{\text{F}} = 188.6$  MHz. Therefore, many MR tomographs can use their  $^1\text{H}$  hardware as amplifiers, filters, transmitters, etc. for  $^{19}\text{F}$  MR. The wide tuneable coil must enable tuning to both  $^1\text{H}$  and  $^{19}\text{F}$  resonances.

In this work, we describe a new design for a sensitive radiofrequency volume coil (volume of interest ~ 100 ml) intended for in vivo  $^1\text{H}/^{19}\text{F}$  MR whole-body imaging and spectroscopy in small rodents using a 4.7 T experimental spectrometer. The  $^1\text{H}/^{19}\text{F}$  coil described herein – a low pass birdcage coil (LPBC) – is intended for preclinical research. The special feature of the LPBC structure is that it can easily and continuously change its length (described below). The resonance frequency of LPBC is determined by inductance  $L$  and capacity  $C$  of the LPBC parts (Eq.2). By changing the length of the coil rungs, the resonance frequency ( $f$ ) can also be manipulated effectively and evenly. This solution (Fig. 1a) maintains good homogeneity over the entire tuning range and enables broader frequency tuning (>25%) than the  $^1\text{H}/^{19}\text{F}$  coil tuning range (6%). The small capacity of the tuning capacitor is used for fine-tuning only (Fig. 1).

From a circuit and construction point of view, the main difference of our approach compared to a classical LPBC construction is to replace capacitors in the rungs with overlapping metal tapes. These form a transmission line resonator (TLR) [12] separated by an FR-4 dielectric in a sliding manner (Figs. 1a and 1b show the yellow rungs sitting on top of the FR-4 substrate).

$$C = \epsilon \frac{S}{l} \quad [F, F \times m^{-1}, m^2, m]$$

**Eq. 1: Dependence of capacity on dimensions**

The overlap can be changed by sliding the parts of the cage against each other along the longitudinal axis of the coil. Changes in rung length and overlap also correspond to changes in rung inductance and capacity (Eq. 1). The rung inductance changes are very small with respect to capacitance changes. Parts of the rungs have almost the same  $L$  inductance, but changing the  $C$  capacity between rungs causes the resonance frequency of the coil to change according to Eq. 2:

$$f = \frac{1}{2\pi\sqrt{LC}} \quad [Hz, H, F]$$

**Eq. 2: Thomson’s resonant formula**

Replicating the TLR on a cylindrical surface leads to the formation of a birdcage-like structure, which has the same properties as a birdcage with respect to the RF field (Figs. 1a and 4). The concept behind TLR is to reduce the requirements of non-magnetic components and to free up space around coils resisting measurement. The coil consists of 12 rungs (ensuring sufficient homogeneity of the  $B_1$  RF field) and two end rings that connect the 12 rungs in one conductive unit. The cage is coupled to the tuning transformer for fine-tuning of the resonance frequency. This transformer is formed by a tuning circle at a distance of 4 mm from the coil end ring (Figs. 1a and 1b). The resonance frequency can be set precisely within a narrow range using the capacitive coupling between the two circles. This precise tuning method is used in standard volume coils.

The coil is of good homogeneity and uniquely constructed to facilitate easy tuning for  $^1\text{H}/^{19}\text{F}$  MR, as previously tested (on phantoms containing various concentrations of a fluorinated compound) by MR relaxometry, imaging and spectroscopy. The coil has also been applied to  $^1\text{H}$  in vivo MR imaging of liver in healthy and tumour-bearing mice. It has also been used in spectroscopy and relaxometry  $^{19}\text{F}$  experiments to measure phantom spectra.

## II. Methodology

### 2.1 Electromagnetic field simulation

Experimental MR system with a magnetic field strength of 4.7 T (Bruker Biospec MRI GmbH, Ettlingen, Germany).

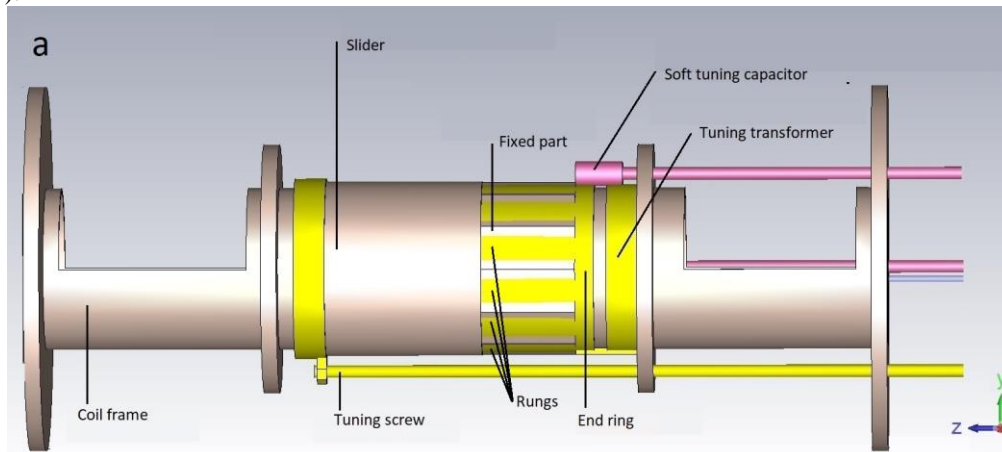


**Fig. 1: Visualization of simulated structure without shield (a)**

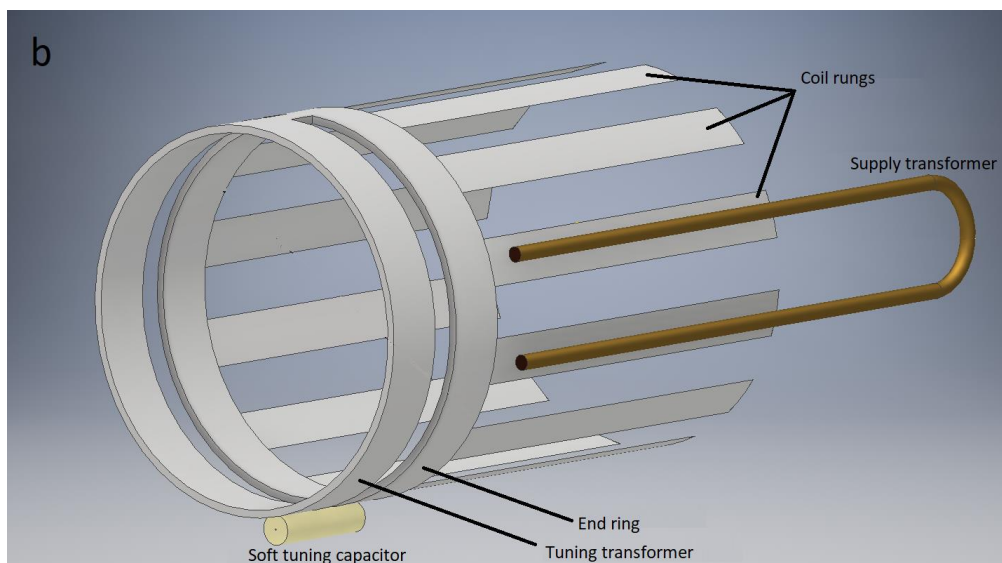


**Fig. 1: Detail of slider with marked important parts (b)**

Coil parameters were optimised using a numerical simulation tool on CST software (CST Studio Suite 2016 Student Edition, Dassault Systèmes, France). CST allows 3D circuit models to be easily created, setting parameters for interactions between models and free space. A copper-like material ( $G_{\text{Cu}} = 58,1 \cdot 10^6 \text{S} \cdot \text{m}^{-1}$ ,  $\epsilon^r = 1$ ,  $\mu^r = 1$ ) was used to simulate the coil conductors: FR-4 ( $G_{\text{FR4}} = 0 \text{S} \cdot \text{m}^{-1}$ ,  $\epsilon^r = 4,4$ ,  $\mu^r = 1$ ) is a commonly used substrate for printed board production. We used it to simulate a dielectric, with air used to simulate the surrounding environment. These material constants are considered linear and independent of frequency and field intensity. The spatial distribution of the alternating  $B_1$  electromagnetic field was obtained by calculating Maxwell equations (Figs. 2a and 2b). Alternating currents 1 A/200 MHz and 1 A/188 MHz were used for the simulation. The coil dimensions were optimised by simulating an intensity curve of the  $B_1$  field with one maximum in the centre (Fig. 1c). Most birdcage coils are constructed to suit a curve, with two intensity maxima of  $B_1$  corresponding to the longest volume of the homogeneous  $B_1$  field [2]. The one-maximum design

provides greater sensitivity in the isocentre. However, this increased sensitivity also reduces the homogeneous area along the z-axis (see Figs. 2b and 2d).

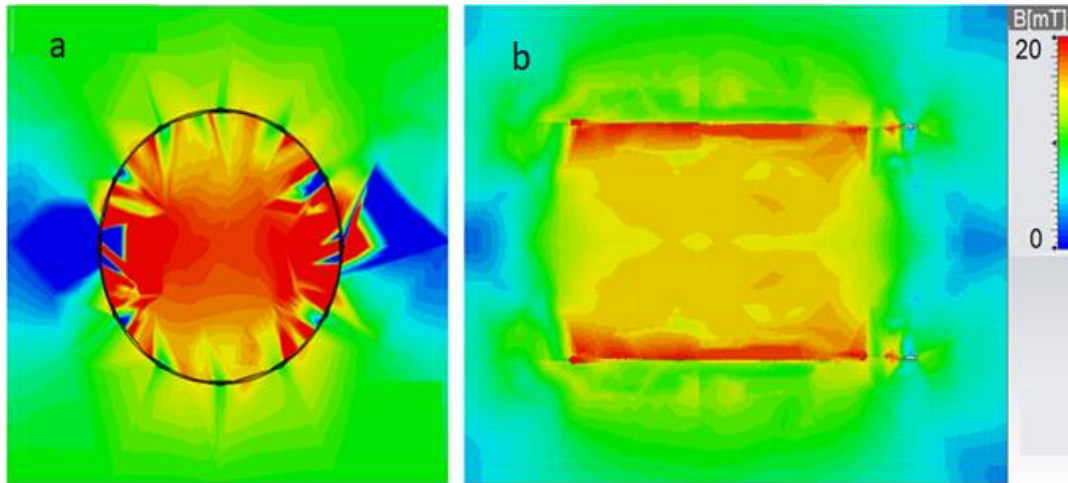


**Fig. 2: Transversal simulation of  $B_1$  field in CST (a), Coronal simulation of  $B_1$  field in CST (b)**

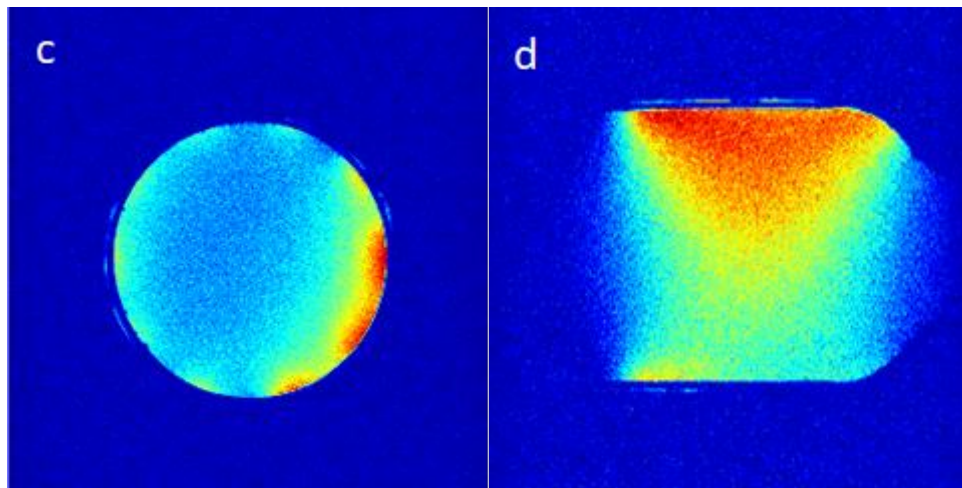


**Fig. 2: Measured transversal  $B_1$  field (c), Measured coronal  $B_1$  field (d)**

The simulated working area of the coil is defined by a border for the 3 dB RF  $B_1$  field cut-off, situated 27.5 mm from the coil centre. For this reason, the length of the measured sample should not exceed 55 mm (Fig. 2b).

## 2.2. Design and coil construction

The coil was constructed in the laboratories of the Technical University of Liberec (TUL). The mechanical body was drafted using Inventor 2016 (Autodesk Inc., USA) and constructed from polycarbonate (PC) using 3D printing technology. To construct the electrical circuits, non-magnetic Exxelia capacitors (Exxelia, France) were used. The printed circuit board structures were etched from a 50  $\mu\text{m}$  copper foil based on a 0.1 mm FR-4 substrate. Since a substrate is flexible, the sheet can be easily formed into cylindrical shape. The dimensions of the coil were chosen to meet the requirements of a whole-body mouse MRI, featuring sensors for breath measurement, temperature, application of anaesthesia for in vivo experiments, and installation of water heating for the rodent body (length 55 mm, diameter 49 mm). The coil itself consists of two end circles, from which 12 rungs extend in the “z” direction. The rungs are free-ended without an endpoint for the end ring, similar to a simple antenna dipole (Fig. 1b). Other rungs of the same geometry overlap the latter at a distance of 0.1 mm set by the FR-4 substrate thickness, forming a set of variable capacitors. Capacities in rungs can be adjusted by changing the cage length. This construction forms one coil from the two galvanic separated parts. Because the coil has an LPBC design, capacities are situated in the longitudinal rungs according to the scheme shown in Fig. 3. Changing the length of all twelve rungs simultaneously changes the operating frequency across the coil operating volume without local field deviations in the  $B_1$  field.

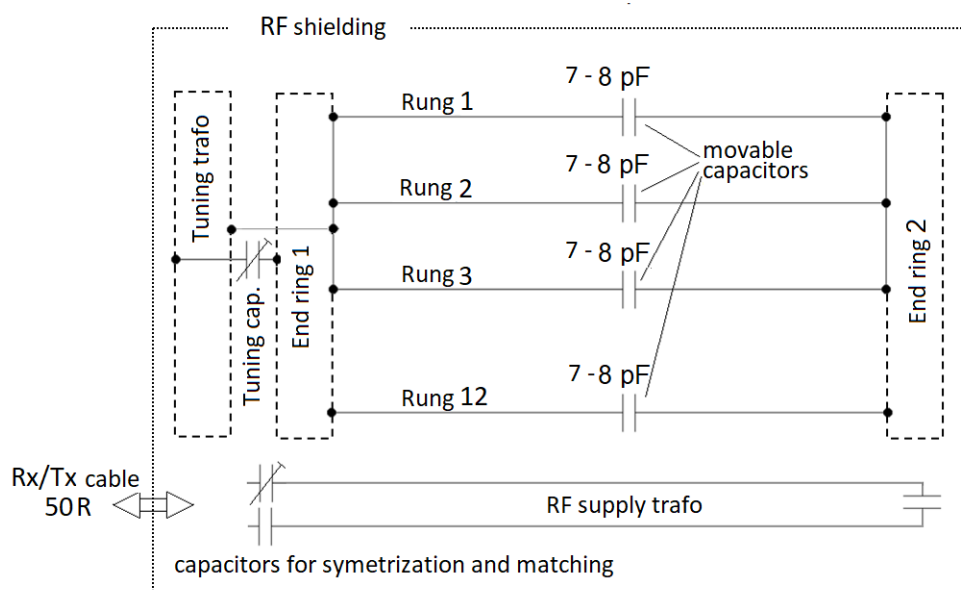


**Fig. 3: Complete electric schema of radiofrequency volume coil**

Changing the cage length makes it possible to tune the operating frequency of the entire coil in all rungs at the same time to a high level of efficiency. Since this tuning method is relatively rough, one more tuning transformer was added to form a circle similar to the end ring located further along the “z” axis direction (Figs. 1a and 1b). At one side, the tuning circle is directly connected to the end ring, and on the opposite side to a capacitive trimmer within an arrangement of 1-8 pF. By changing the trimmer value, the operating frequency can be fine-tuned precisely to  $\pm 1.2$  MHz. The galvanic connection of the end ring and tuning transformer is rotated 90° to the supply transformer (Figs. 1a and 1b).

In a classical design, 29 discrete capacitors would be needed for a similar 12-rung coil. For the design described in this paper, only 4 capacitors (two variables) are needed. The price of the coil is significantly less as a result of the lower component count. These capacitors help to adjust the field homogeneity of the supply transformer, enable impedance matching, and fine-tune the resonance frequency. As the coil has a TLR design, a uniform distribution of the electric field is achieved around the individual coil rungs, with a lower voltage value on the dividing capacities. The lower voltage value leads to the reduction of electric field losses and the improvement of coil quality (Q) [2].

For the  $^{19}\text{F}$  mode, the coil length must be shortened to correspond with the  $^1\text{H}$  mode to increase capacity between rungs and decrease the resonance frequency. To tune from  $^1\text{H}$  to  $^{19}\text{F}$  mode, the coil length is shortened by 2 mm by turning the adjusting screw to which the sliding part of the cage is welded. The precise length of the cage depends on the volume of the sample and its conductivity in particular. In the case of a standard 15 ml test tube with 1 mol/l concentration of NaF, the length of the coil for the  $^1\text{H}$  resonance and the  $^{19}\text{F}$  resonance is 54.6 mm and 52.8 mm, respectively. In the case of a standard 30 ml test tube, the settings would be  $^1\text{H} = 54.4$  mm and  $^{19}\text{F} = 52.5$  mm.

### 2.3 MR experiments

MR experiments were performed on a 4.7 T MR spectrometer (Bruker Biospec, Ettlingen, Germany). The magnet is equipped with commercial, shielded gradient coils at a maximum magnetic gradient of 200 mT/m with a deviation of  $<4\%$  at  $\pm 40$  mm from the isocentre. The internal usable diameter of the gradient system around the isocentre is 120 mm. For coil homogeneity testing, the signal intensity profile was measured with a  $^1\text{H}$  MR imaging sequence and a gradient echo sequence (fast low-angle shot (FLASH) magnetic resonance imaging) using a  $10^\circ$  flip angle (FA) (Figs. 2c,d). To check the  $^{19}\text{F}$  sensitivity of the coil, the tubes with different concentrations of NaF (0.5, 0.25, 0.1 and 0.05 M; volume 0.5 ml) were measured by  $^{19}\text{F}$  MR imaging (FLASH sequence, echo time / repetition time (TE/TR) = 130/2500 ms, 32 acquisitions) and  $^{19}\text{F}$  MR spectroscopy using a standard single-pulse sequence based on the following parameters: TE/TR = 3.8/1069 ms, 32 acquisitions, FA =  $30^\circ$  and scan time 34 s. A spectrum of NaF solution was measured at 188 MHz for a bandwidth of 100 ppm. The  $^1\text{H}$  mode was also tested in an in vivo experiment with mice. A standard MR contrast agent, Gadovist (bolus of 50  $\mu\text{l}$ , concentration 1M), was intravenously applied into the tail vein of the mouse for contrast enhancement in the liver. The mouse liver and kidney were scanned using a FLASH sequence (TE/TR = 3.7/130

ms, 32 acquisitions, scan time 17 min and 44 s). SNR was calculated from images as a ratio of the liver signal, with 4 circles from image corners as noise (Eq. 4).

### III. Results

#### 3.1 Coil parameters

The simulations of projections in Figs. 2a and 2b demonstrate good homogeneity of the RF field, especially in the middle of the coil. There is a stronger horizontal field line in the transversal section, an inhomogeneity that can be compensated for by using a more advanced coil construction called a quadrature excitation. This helps create an additional field component in the vertical direction of the rotating field (not implemented here). Artefacts on the cross-section of the coil (Figs. 2a, 2c) around the wires are characteristic of all birdcage coils. They can be reduced by increasing the number of rungs but at the expense of higher structural requirements. The simulation of fields in the coronal section (Fig. 2b) reveals inhomogeneities in the area of the end rings. On the right, there is an evident increase in inhomogeneity in the area of the tuning transformer. Thus, it is not advisable to construct coils with a strongly coupled tuning transformer, since the inhomogeneous magnetic field in the volume of interest (VOI) increases, in turn leading to inhomogeneities in MR images. The transformer is therefore only suitable for tuning within a resonance frequency range <1%. The simulation results clearly show the distribution of the B<sub>1</sub> field (Figs. 2a, 2b).

The coil is about 55 mm long in <sup>1</sup>H mode, providing one local maximum intensity in the B<sub>1</sub> RF field at the centre of the coil (Fig. 2d). The coil diameter in <sup>1</sup>H mode is 49 mm, while the geometric ratio length/coil diameter is ~ 1.12. For <sup>19</sup>F mode, the ratio is similar at ~ 1.10, with the exact value depending on the load. In cases where the homogeneous area needs to be lengthened, the optimum coil length is 81 mm for <sup>1</sup>H mode. However, in this case, that would decrease the absolute value of the MR signal received as well as the sensitivity of the coil.

The coil tuning range is mechanically limited from 180 MHz to 210 MHz. While tuning, there are 4 near peaks in the spectrum of resonance modes. The lowest frequency mode must always be chosen to achieve peak coil performance. If the higher resonance mode is tuned, the maximum energy is not concentrated in the coil. Therefore, at higher harmonic modes, the MR signal is weakened and the RF field deformed, resulting in unwanted artefacts in MR images [2]. Quality factor Q was determined from the bandwidth (B<sub>w</sub>) for the given frequency (f<sub>0</sub>) with an amplitude drop of -3 dB according to equation 3:

$$Q = \frac{f_0}{B_w} \quad [-, Hz, Hz]$$

#### Eq.3: Formula for electric resonance quality

The quality factor calculated for the unloaded coil was: Q<sub>19F (4.7T)}</sub> = 331 and Q<sub>1H (4.7T)}</sub> = 328. The qualitative parameters of these types of Q coils, as previously described in the literature [2], are coils with one working frequency only, comparable to those measured on the coil described here. However, the design of our coil also enables broad frequency tuning with comparable parameters of field quality and homogeneity.

The coil is designed for both exciting and receiving MR signals (Tx/Rx coil). A signal transfer between the coil and the cable is realised with a high-frequency supply transformer (Fig. 1b), which lies parallel to the cage rungs. The transformer supply loop is connected via a capacitive trimmer. This solution allows the loop to match to the 50 Ω cable and thus prevents unwanted reflections of waves or any associated reduction in signal intensity. Reflection value S<sub>11</sub> must be less than -50 dB. The other side of the supply loop is connected by a fixed capacitor (Fig. 3), which improves the symmetry of the RF wave and helps suppress the effects of disturbances and the influence of surface currents on the coaxial cable.

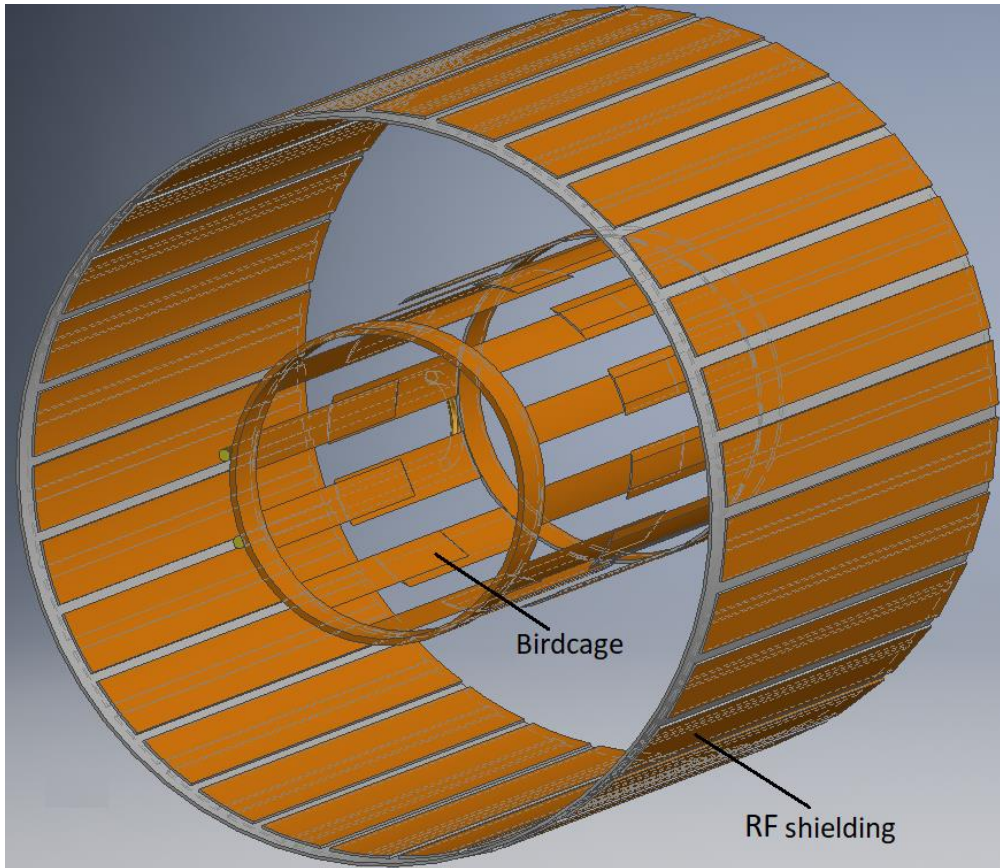


**Fig.4: Coil structure with RF shielding**

The complete coil system and RF circuits are separated by RF shielding (Fig. 4), which has the effect of cancelling the coupling between the gradient coils and the RF coil. This in turn improves the homogeneity and stability of the  $B_1$  RF field inside the coil. The shielding is made of copper strips on the FR-4 board. The isolating gaps between the strips divide the large copper area of the cylinder surface in a large number of smaller strips (Fig. 4). This solution reduces the dimensions of the contiguous copper surface and reduces the influence on low-frequency EM fields such as gradient pulses, which generate eddy currents in the contiguous conducting surface, and other magnetic field inhomogeneities. Conductivity for the RF field is maintained due to the mutual capacity of the individual strips, causing only a minor reactance in the RF field.

The construction of the coil presented here facilitates a large frequency tuning range via changes in coil cage geometry, especially with regard to length. Theoretically, it is possible to achieve a tuning frequency range  $>25\%$ . However, for user-friendly operation, the tuning range for the  $^1\text{H}/^{19}\text{F}$  coil is mechanically limited to 6% to allow enough reserve and cover the Larmor frequencies  $f_{19\text{F}(4.7\text{T})} = 188 \text{ MHz}$  and  $f_{1\text{H}(4.7\text{T})} = 200 \text{ MHz}$ . For a comparison of the novel design of our coil with the classic birdcage coil, see Table 1 [2].

**Tab. 1: Comparison of standard volume coil and new designed coil**

	Coil with movable geometry	Classic MR coil
Quality factor (Q)	328-331	340
Relative tuning	$>6\%$	2%
Stuff price	\$500	\$5,000

### 3.2 MR experiment

$^1\text{H}$  MR imaging boasts a high SNR and is adept at visualising  $B_1$  field homogeneity. Based on the homogeneity of the image, which occupies a considerable part of the cross-section of the coil, the uniformity of excitation of the sample and the homogeneity of the  $B_1$  field within the coil can be deduced. The whole coil volume in Figs.2c and 2d shows highly homogeneous  $^1\text{H}$  images. The recommended volume of the coil for providing high-image performance is  $103.7 \text{ cm}^3$ . The inhomogeneities of  $B_1$  compared with simulations in Figs. 2a and 2b are probably due to the conductivity of the water measured, since the simulations in Figs. 2a and 2b were calculated without a load.

$$SNR = 0,655 \frac{I_{sig}}{\sigma}$$

**Eq. 4: Formula for SNR calculation**

To test fluorine mode, a 0.5 ml volume solution of NaF was used at different concentrations (see Table 2). This solution is used due to the high content of fluorine nuclei and non-negligible electrical conductivity, which is comparable to the conductivity of the physiological solution or of the mammalian tissue. SNR values were calculated according to Eq. 4.

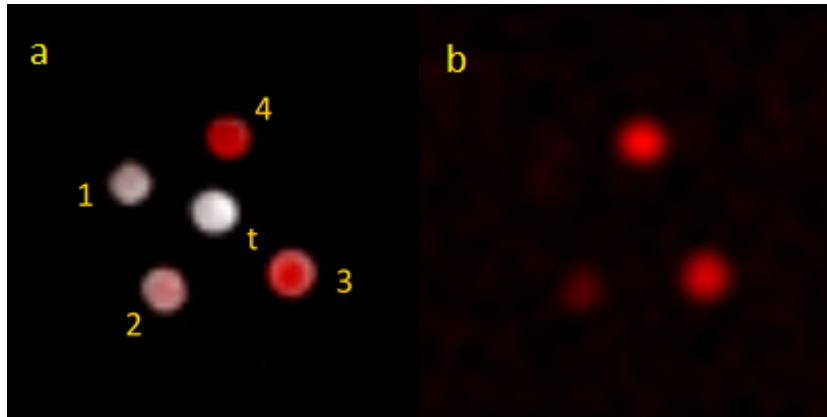


**Fig. 5: Fluorine and hydrogen test images. Overlapped <sup>1</sup>H and <sup>19</sup>F images with different concentrations of fluorine nuclei (1 = 0.05 M, 2 = 0.1 M, 3 = 0.25 M, 4 = 0.5 M, t = test tube, water only) (a), <sup>19</sup>F image with different concentrations of fluorine <sup>19</sup>F (b)**

To verify the function of the <sup>19</sup>F and <sup>1</sup>H mode, transversal MR images of small tubes were measured. The tubes were uniformly distributed in the centre of the coil, containing NaF water solutions at various concentrations. A reference tube (R) containing water but without NaF was located in the centre to test for the independence of the fluorine and hydrogen channels.

Fig. 5a shows an <sup>19</sup>FMR image overlaid on a reference <sup>1</sup>H image. Fig. 5b shows the <sup>19</sup>F signal only, with each tube represented by a circle of different brightness to indicate the intensity of the <sup>19</sup>F signal received and reflect different concentrations of <sup>19</sup>F. Intensity is linearly proportional to the number of fluorine molecules, as previously theorised [13]. The dependence of the SNR to the concentration of the solution is given in Table 2.

**Tab. 2: Dependence of SNR to concentration**

Phantom	Concentration	Nucleus	SNR
1	0,05M/l	1,055*10 <sup>19</sup>	78
2	0,1M/l	3,11*10 <sup>19</sup>	144
3	0,25M/l	7,52*10 <sup>19</sup>	352
4	0,5M/l	1,5*10 <sup>20</sup>	743

For spectroscopy and relaxometry experiments, good B<sub>1</sub> homogeneity is required for uniform excitation and to achieve a consistent flip angle throughout the sample volume. Our results from the B<sub>1</sub>field mapping suggest that the coil is suitable for MR spectroscopy and relaxometry experiments. The modulus of spectra values is shown in Fig 6. Homogeneity of the B<sub>1</sub> field was confirmed by a narrow half-width of spectra – 150 Hz (corresponding to 0.79 ppm) – which is lower than the half-width obtained from the same sample measured by the surface coil (data not shown).



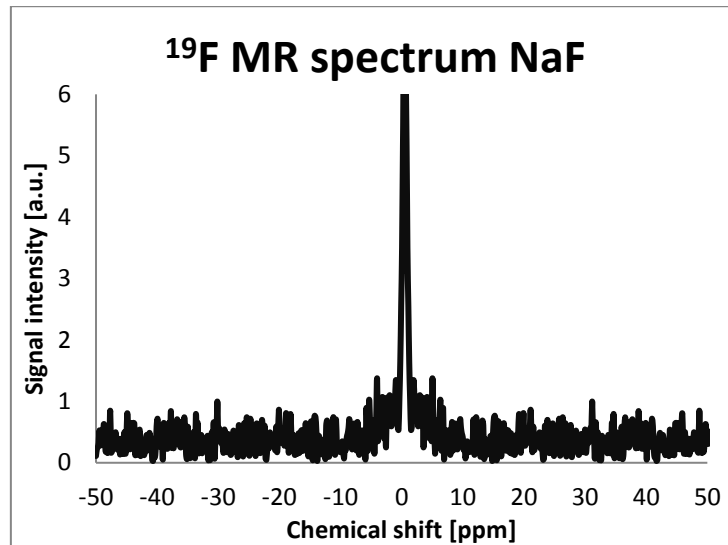


Fig. 6: Spectrum of NaF measured with new coil

To verify the performance of  $^1\text{H}$  mode under in vivo conditions, an in vivo MR measurement of a mouse liver was performed. Our experiment demonstrated that the coil dimensions are suitable for whole-body imaging of mice, while providing better homogeneity and sensitivity than commercially available coils. It is also essential to insert a breathing monitor along with heating water hoses into the coil to ensure proper in vivo measurements. The SNR of the liver is shown in Fig. 7.

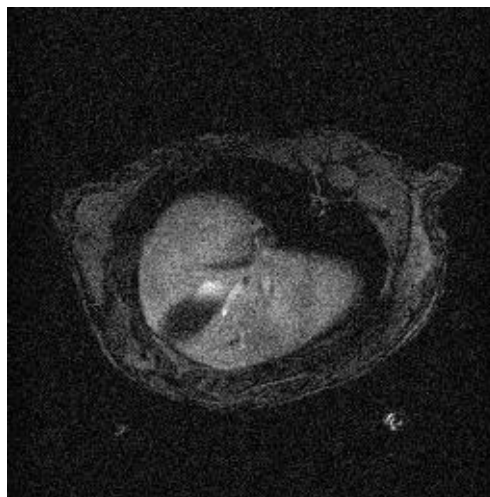


Fig. 7: In vivo mouse liver measurement

Our results show that the dual volume  $^1\text{H}/^{19}\text{F}$  coil is comparable to commercial coils designed for measurement only with single specific nuclei. The main coil features are simple tuning and robustness, which are important for high-quality, repeatable and reproducible results for in vivo experiments.

#### IV Conclusion

The wide tuneable volume  $^1\text{H}/^{19}\text{F}$  coil is a suitable tool for high-quality anatomical imaging of small rodents and  $^{19}\text{F}$ -probe tracking. The ability of the coil to work in both resonance modes facilitates and accelerates  $^{19}\text{F}$  MR experiments in cases where a reference  $^1\text{H}$  MR image is required. Compared to other dual  $^1\text{H}/^{19}\text{F}$  coils [14], the unique design of the coil presented here is characterised by one resonance peak formation only. This results in better resonance tuning and, consequently, a higher SNR for MR images. A standard dual  $^1\text{H}/^{19}\text{F}$  coil [14] has  $Q_{\text{unloaded}} = 192$ , but our coil has a much higher unloaded Q factor of  $Q_{^1\text{H}/^{19}\text{F}} = 331/328$ . Moreover, the coil possesses a large and highly homogeneous field of view, enabling whole-body scans of small rodents. Another advantage of this innovatively designed coil is its lower cost compared to coils that rely on capacitors with lumped elements, allowing it to be constructed even in the most basic of laboratories.

## V Acknowledgements

The work was supported by TUL fund SGS-21332, GAČR project P205-16-03156S, the Czech Science Foundation (project number 19-03207S), and the Ministry of Health of the Czech Republic (grant CZ-DRO, IN00023001).

All intellectual property rights are reserved.

## References

- [1]. Doty FD (2007) Radio frequency coil technology for small-animal MRI. *NMR Biomed*
- [2]. Mispelter J, Lupu M, Briguet A (2015) *NMR Probeheads for Biophysical and Biomedical Experiments: Theoretical Principles and Practical Guidelines* (2<sup>nd</sup> Edition). Imperial College Press 257–259
- [3]. Konstandin S, Schad LR (2014) 30 years of sodium/X-nuclei magnetic resonance imaging. *Magn Reson Mater*
- [4]. Peterson KL, Srivastava K, Pierre VC (2018) Fluorinated paramagnetic complexes: sensitive and responsive probes for magnetic resonance spectroscopy and imaging. *Front Chem* 6
- [5]. Srinivas M, Heerschap A, Ahrens ET, Figdor CG, deVries IJM (2010) <sup>19</sup>F MRI for quantitative in vivo cell tracking. *Trends Biotechnol* 28(7):363–370
- [6]. Ahrens ET, Helfer BM, O'Hanlon CF, Schirda C (2014) Clinical cell therapy imaging using a perfluorocarbon tracer and fluorine-19 MRI. *Magn Reson Med* 72(6):1696–1701 <https://doi.org/10.1002/mrm.25454>
- [7]. Du WJ, Xu ZQ, Nystrom AM, Zhang K, Leonard JR, Wooley KL (2008) F-19- and fluorescently labeled micelles as nanoscopic assemblies for chemotherapeutic delivery. *Bioconjugate Chem* 19(12):2492–2498
- [8]. Tirotta I, Dichiarante V, Pigliacelli C, Cavallo G, Terraneo G, Bombelli FB, Metrangolo P, Resnati G (2015) <sup>19</sup>F magnetic resonance imaging (MRD): from design of materials to clinical applications. *Chem Rev* 1106–1127
- [9]. Ruiz-Cabello J, Barnett BP, Bottomley PA, Bulte JW (2011) Fluorine (<sup>19</sup>F) MRS and MRI in biomedicine. *NMR Biomed* 24(2):114–129
- [10]. Yu JX, Hallac RR, Chiguru S, Mason RP (2013) New frontiers and developing applications in <sup>19</sup>F NMR. *Prog Nucl Magn Reson Spectrosc* 70:25–49
- [11]. Weissleder R. (2010) *Molecular Imaging*, PmpH-USA, 391–407
- [12]. Nezhadian SH (2017) A flexible transceiver array employing transmission line resonators for cardiac MRI at 7 T. *Medical Physics* 89–107
- [13]. Jirak D, Galisova A, Kolouchova K, Babuka D, Hruby M (2019) Fluorine polymer probes for magnetic resonance imaging: quo vadis? *MAGMA*. 32(1):173-185
- [14]. Villa-Valverde P, Rodríguez I, Padró D, et al. (2019) A dual <sup>1</sup>H/<sup>19</sup>F birdcage coil for small animals at 7T MRI. *MAGMA* 32(1):79-87

M. Vít" Construction Of A Wide tuneable Volume Coil For Small-Animal MR Imaging"  
International Journal of Engineering Science Invention (IJESI), Vol. 08, No. 07, 2019, PP 08-17